Mon. Not. R. Astron. Soc. **000**, 1–10 (2013) Printed 30 September 2014 (MN LATEX style file v2.2)

On the asymptotic acoustic-mode phase in red-giant stars and its dependence on evolutionary state

Jørgen Christensen-Dalsgaard[1⋆], Victor Silva Aguirre[1], Yvonne Elsworth[2,1], Saskia Hekker[3,1]

[1] *Stellar Astrophysics Centre, Department of Physics and Astronomy, Aarhus University, DK–8000 Aarhus C, Denmark,*
[2] *School of Physics & Astronomy, University of Birmingham, Edgbaston Park Road, West Midlands, Birmingham B15 2TT, UK,*
[3] *Max-Planck-Institut für Sonnensystemforschung, Justus-von-Liebig-Weg 3, 37077 Göttingen, Germany*

arXiv:1409.7949v1 [astro-ph.SR] 28 Sep 2014

Received 30 September 2014/ Accepted 30 September 2014

ABSTRACT

Asteroseismic investigations based on the wealth of data now available, in particular from the CoRoT and *Kepler* missions, require a good understanding of the relation between the observed quantities and the properties of the underlying stellar structure. Kallinger et al. (2012) found a relation between their determination of the asymptotic phase of radial oscillations in evolved stars and the evolutionary state, separating ascending-branch red giants from helium-burning stars in the 'red clump'. Here we provide a detailed analysis of this relation, which is found to derive from differences between these two classes of stars in the thermodynamic state of the convective envelope. There is potential for distinguishing red giants and clump stars based on the phase determined from observations that are too short to allow distinction based on determination of the period spacing for mixed modes. The analysis of the phase may also point to a better understanding of the potential for using the helium-ionization-induced acoustic glitch to determine the helium abundance in the envelopes of these stars.

Key words: Stars: atmospheres – stars: evolution stars: oscillations – convection

1 INTRODUCTION

The observations of stellar oscillations carried out by the CoRoT (Baglin et al. 2009) and *Kepler* (Borucki et al. 2010) missions have revolutionized asteroseismology, by providing extensive photometric data of high quality for a large number and great variety of stars. This includes a very substantial number of stars showing solar-like oscillations, i.e., modes that are intrinsically damped and excited stochastically by vigorous near-surface convection.

A particularly interesting case are the red-giant stars, representing late evolutionary phases of low- and moderate mass-stars (see, for example, Kippenhahn et al. 2012 for a general overview of stellar evolution; for a detailed discussion of the properties of red giants, see Salaris et al. 2002). After completing central hydrogen fusion stars evolve towards lower effective temperature $T_{\rm eff}$, before ascending the red-giant branch (RGB) with increasing luminosity and nearly constant $T_{\rm eff}$. This evolution is driven by the formation of a helium core whose mass grows through the continued hydrogen fusion in a shell around the core, while the core radius decreases. This is accompanied by a strong increase in the surface radius. When the temperature in the core becomes sufficiently high, fusion of helium to carbon and oxygen sets in. For stars of mass lower than around $1.8\,{\rm M}_\odot$ the pressure in the inert helium core is dominated by degenerate electrons and helium fusion starts as a run-away process, the so-called helium flash, leading to a complex and poorly modelled evolution, before the star settles down to quiescent helium fusion. For higher-mass stars the core is non-degenerate, and helium fusion starts in a more regular fashion. The ignition of helium leads to an expansion of the core and a corresponding contraction of the envelope, decreasing the surface radius and hence the luminosity, with a slight increase in $T_{\rm eff}$. In both cases the hydrogen-fusing shell outside the helium core continues to contribute a substantial fraction of the total surface luminosity. Stars in the core helium-fusion phase are often referred to as 'clump' stars, from the location of such stars in the so-called 'red clump' in colour-magnitude diagrams of open clusters. For field stars, as opposed to cluster stars, it is very difficult to distinguish between RGB and clump stars based just on their observed surface properties, given the scatter induced, e.g., by differences in metallicity.

To ascertain the diagnostic potential of the observed

⋆ E-mail: jcd@phys.au.dk

© 2013 RAS

oscillations it is necessary to consider the properties of the observed oscillation modes (for a detailed discussion of these properties and asteroseismic diagnostics, see Aerts et al. 2010). In red giants the compact core gives rise to a very high local gravitational acceleration and hence buoyancy frequency in the deep interior of the star. For non-radial modes, with spherical-harmonic degree l greater than 0, this leads to a dense spectrum of trapped internal gravity waves, or g modes, in the core. In the envelope the modes behave as acoustic waves, or p modes. Thus all non-radial modes have a mixed character, with g-mode behaviour in the core and p-mode behaviour in the envelope. At certain frequencies there is a resonance with the acoustic behaviour in the envelope, leading to modes of predominantly p-mode character, with larger amplitudes in the envelope than in the core. Owing to their lower inertia such modes are easier to excite by the near-surface convection and hence are generally more visible in the observations (e.g., Dupret et al. 2009). To these non-radial modes must be added the spherically symmetric, or radial, modes with $l = 0$ which are of purely acoustic character.

A major early breakthrough from the CoRoT observations of red giants was the identification of non-radial acoustically dominated modes (De Ridder et al. 2009). Remarkably, this was soon followed by the detection of additional modes of degree $l = 1$ with a substantial g-mode component (Beck et al. 2011). Such modes are characterized by the period spacing between adjacent modes, which is determined by the buoyancy frequency in the deep interior of the star and hence provides a diagnostics of conditions in the core. As a very important result it was shown by Bedding et al. (2011) and Mosser et al. (2011a) that the period spacing is substantially higher in clump stars than in RGB stars, providing a first clear observational separation, applicable to individual stars, between these two classes. This obviously requires a clear observational identification of the g-dominated modes. Such an identification has been possible on the basis of observations over several years that were obtained during the nominal *Kepler* mission (e.g., Mosser et al. 2012; Silva Aguirre et al. 2014). However, the shorter duration of the observations in the K2 extension of *Kepler* (Howell et al. 2014) and for the TESS mission (Ricker et al. 2014) makes unlikely a detailed analysis of g-dominated modes.

Here we concentrate on the acoustically dominated modes which, as mentioned above, are probably those that are most easily observable. Acoustic modes satisfy an approximate asymptotic relation which can be written

$$\nu_{nl} \simeq \Delta\nu \left(n + \frac{l}{2} + \epsilon \right) - d_{0l} \tag{1}$$

(e.g., Tassoul 1980), where ν_{nl} is the cyclic frequency of the mode of radial order n and degree l. The separation between modes of the same degree and adjacent order (the so-called large frequency separation) is approximately given by

$$\Delta\nu \simeq \left(2 \int_0^{R_*} \frac{\mathrm{d}r}{c} \right)^{-1} , \tag{2}$$

where c is the adiabatic sound speed and the integral is over distance r to the centre of the star, extending to a suitable value R_* near the surface of the star. In equation (1) ϵ is a phase which, as extensively discussed below, depends on frequency and is probably predominantly determined by the properties of the near-surface layers of the star, and d_{0l} is a small correction. This expression can relatively simply be derived for main-sequence stars where d_{0l} provides a useful diagnostic of the evolutionary stage (e.g., Christensen-Dalsgaard 1984, 1988; Ulrich 1986). The applicability of equation (1) to red giants is perhaps less obvious, in the light of their compact core, but is clearly shown both by stellar models and by observations of red giants (e.g., De Ridder et al. 2009; Bedding et al. 2010; Huber et al. 2010), leading to the introduction of the so-called 'universal pattern' (Mosser et al. 2011b; see, however, Stello et al. 2014).

It follows from simple homology relations that $\Delta\nu$ scales as the square root of the mean density of the star,

$$\Delta\nu \propto \left(\frac{M}{R^3} \right)^{1/2} \tag{3}$$

(Ulrich 1986). Thus determination of $\Delta\nu$ from observations provides a strong constraint on the global properties of the star, although corrections to this scaling may be required, as discussed, e.g., by White et al. (2011) and Miglio et al. (2012). However, as a result of the frequency dependence of ϵ the actual separation between adjacent modes,

$$\Delta\nu_{nl} \equiv \nu_{n+1\,l} - \nu_{nl} \simeq \Delta\nu[1 + \epsilon(\nu_{n+1\,l}) - \epsilon(\nu_{nl})] , \tag{4}$$

in general differs from the asymptotic separation $\Delta\nu$. This must be taken into account when the scaling relation (3) is applied to values of $\Delta\nu$ estimated from the observed frequencies. On the other hand, the frequency dependence of $\Delta\nu_{nl}$ provides diagnostics of the outer layers of the star, including the envelope helium abundance (e.g., Miglio et al. 2010).

A second important global asteroseismic diagnostics is the frequency $\nu_{\max}$ where the power density is maximum. This can be determined relatively accurately by fitting, e.g., a Gaussian to the envelope of power. It has been found observationally (e.g., Brown & Gilliland 1994; Stello et al. 2008), with some theoretical support (Belkacem et al. 2011), that $\nu_{\max}$ scales as the acoustic cut-off frequency in the stellar atmosphere, leading to

$$\nu_{\max} \propto \frac{M}{R^2} T_{\rm eff}^{-1/2} , \tag{5}$$

where $T_{\rm eff}$ is the effective temperature. Given an observational determination of $T_{\rm eff}$ the radius and mass of a star can be determined from observed values of $\Delta\nu$ and $\nu_{\max}$ (e.g., Kallinger et al. 2010).

Kallinger et al. (2012) emphasized the ambiguity of the observational determination of $\Delta\nu$, depending on the selection of modes actually observed, and argued that this might hide significant dependencies of the inferred global asteroseismic parameters. They noted that the large-scale variation of ϵ, reflected in the curvature of the ridges in an échelle diagram, quite generally appears to have a local extremum near $\nu_{\max}$ and hence proposed to base the analysis on just a few radial modes in the vicinity of $\nu_{\max}$. This has the added advantage that these modes may be expected to be the most visible. Specifically, they chose the radial mode, with order $n = n_{\rm c}$, closest to $\nu_{\max}$, and defined the large separation by

$$\Delta\nu_{\rm c} = (\nu_{n_{\rm c}+1\,0} - \nu_{n_{\rm c}-1\,0})/2 . \tag{6}$$

From this they also obtained, as a measure of the phase ϵ,

$$\epsilon_c = \frac{\nu_{n_c 0}}{\Delta\nu_c} \mod 1 \,. \quad (7)$$

Kallinger et al. used this procedure to analyse a large number of red-giant stars for which the evolutionary phases (RGB or clump) were already known from their mixed-mode period spacings. They presented their results in a $(\Delta\nu_c, \epsilon_c)$ diagram. Interestingly, they found evidence for a distinction in ϵ_c between clump and RGB stars at fixed $\Delta\nu_c$, proposing the use of ϵ_c as a diagnostics to identify clump stars based on just the radial-mode frequencies. Given the general preconception that ϵ is determined mainly by the surface layers, and the fact that the structural differences between clump and RGB stars are predominantly in the core, such a significant signature may be somewhat surprising.

Here we analyse the origin of the difference in behaviour between the RGB and the clump model. Section 2 presents results for stellar evolution models of various masses. In Section 3 we analyse the relevant properties of stellar oscillations for models on the RGB and in the clump and relate the difference in ϵ_c to the properties of the convection zones of the two stars; a further analysis of the convection-zone properties is provided in Appendix A. Finally, Section 4 gives a discussion of the results and summarizes our conclusions.

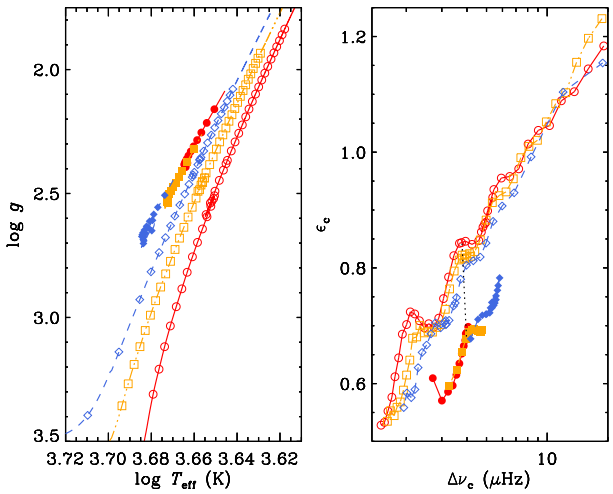

Figure 1. Left panel: evolution tracks on the ascending red-giant branch and the clump for masses of $1\,M_\odot$ (red circles), $1.5\,M_\odot$ (yellow squares) and $2\,M_\odot$ (blue diamonds), computed with the GARSTEC code. Open symbols show models on the red-giant branch, and closed symbols show helium-burning clump models. Right panel: the corresponding large frequency separation $\Delta\nu_c$ and phase ϵ_c, determined in the manner of Kallinger et al. (2012). The models $\mathcal{M}_{\rm RGB}$ and $\mathcal{M}_{\rm RC}$ (cf. Table 1), which are analysed in detail below, are indicated by being connected by the nearly vertical dashed line.

2 STELLAR MODELLING

We computed evolutionary tracks using the GARching STellar Evolution Code (GARSTEC; Weiss & Schlattl 2008). The input physics included the NACRE compilation of nuclear reaction rates (Angulo et al. 1999), the Grevesse & Sauval (1998) solar mixture, OPAL opacities (Iglesias & Rogers 1996) for high temperatures supplemented by low-temperature opacities from Ferguson et al. (2005), the 2005 version of the OPAL equation of state (Rogers et al. 1996) and the mixing-length theory of convection as described by Kippenhahn et al. (2012). Convective overshooting and diffusion of helium and heavy elements were not considered. The parameters of the models were chosen to correspond to a calibrated solar model, including diffusion and settling of helium and heavy elements; this resulted in the convective efficiency $\alpha_{\rm MLT} = 1.791$ and initial abundances by mass of hydrogen and heavy elements of 0.712 and 0.0192. The left panel in Fig. 1 shows resulting evolution tracks for three different masses.

Detailed calculations of individual frequencies were obtained for masses of 1.0, 1.5, and $2.0\,M_\odot$ using the Aarhus Adiabatic Oscillations Package (ADIPLS; Christensen-Dalsgaard 2008). From the frequencies $\Delta\nu_c$ and ϵ_c were determined as described above. The results are shown in the right panel of Fig. 1. There is a clear distinction between the RGB models, at higher ϵ_c, and the clump models, at lower ϵ_c, as also inferred by Kallinger et al. (2012).

In the following we discuss in detail the pair of $1\,M_\odot$ models, $\mathcal{M}_{\rm RGB}$ and $\mathcal{M}_{\rm RC}$, at the same radius and approximately the same $\Delta\nu_c$ on the RGB and in the clump, respectively. The models are connected by the black dashed line in the right panel of Fig. 1. Some details about the models are provided in Table 1.

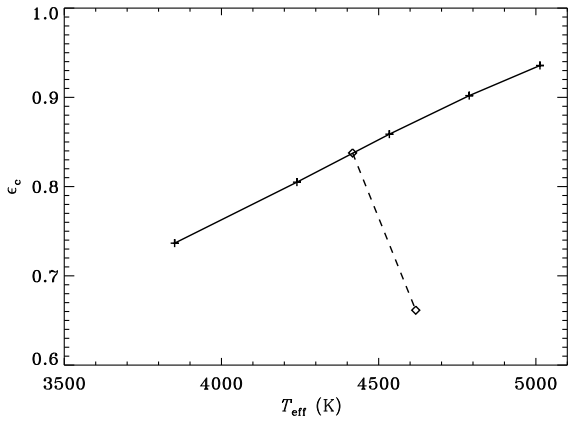

Figure 2. The phase ϵ_c as a function of effective temperature for models at fixed radius ($10.69\,R_\odot$). Solid line: RGB models with $\alpha_{\rm ML} = 1$ (cooler) to 3 (hotter). The diamonds connected by a dashed line show models at fixed $\alpha_{\rm ML}$ (cf. Table 1): the RGB model $\mathcal{M}_{\rm RGB}$ at high ϵ_c and the clump model $\mathcal{M}_{\rm RC}$ at lower ϵ_c.

3 ANALYSIS OF THE ASYMPTOTIC PHASE

Fig. 1 shows a significant difference between ϵ_c between RGB and clump models at fixed $\Delta\nu$ for a given mass, and hence at approximately fixed radius and surface gravity. Here we aim at determining the dominant reason for this difference. One possibility would be that ϵ_c is directly related to the effective temperature, which is the principal difference between the superficial properties of the RGB and clump stars, on the assumption that ϵ_c is predominantly determined by

Table 1. Red-giant ($\mathcal{M}_{\rm RGB}$) and clump ($\mathcal{M}_{\rm RC}$) models, in a $1\,{\rm M}_\odot$ evolution sequence, considered for detailed analysis of $\epsilon_{\rm c}$.

Model	$T_{\rm eff}$ (K)	$R/\,{\rm R}_\odot$	$\Delta\nu_{\rm c}$ (μHz)	$\epsilon_{\rm c}$
$\mathcal{M}_{\rm RGB}$	4417	10.69	3.760	0.8377
$\mathcal{M}_{\rm RC}$	4618	10.69	3.982	0.6615

the stellar surface layers. At the opposite extreme $\epsilon_{\rm c}$ might somehow be directly related to the stellar core, the site of the most fundamental differences between the two types of stars.

To test the assumption that the difference in $\epsilon_{\rm c}$ is related to the difference in effective temperature between RGB and clump we computed a set of evolution sequences for the RGB, varying the mixing-length parameter $\alpha_{\rm ML}$ to change $T_{\rm eff}$ at given radius. We selected models at fixed radius and evaluated $\epsilon_{\rm c}$ as discussed above. In Fig. 2 the results are compared with a pair of models of the same mass and radius on the RGB and the clump, discussed in more detail below. It is evident that the change in $\epsilon_{\rm c}$ from RGB to clump is quite different from the effect expected simply from the change in $T_{\rm eff}$. The effect on $\epsilon_{\rm c}$ must therefore have a more deep-seated origin.

The most dramatic difference between the structure of the RGB and clump model is obviously in the core. It was noted by Roxburgh & Vorontsov (2000, 2003) that the phase in the asymptotic expression for acoustic-mode frequencies does indeed contain a contribution from the core of the star. This can be analysed in terms of the eigenfrequency equation

$$\omega_{nl}T_0 \simeq \pi\left(n+\frac{l}{2}\right)+\alpha_l(\omega_{nl})-\delta_l(\omega_{nl})\;, \tag{8}$$

where $\omega=2\pi\nu$ is the angular frequency, and

$$T_0=\int_0^{R_*}\frac{{\rm d}r}{c} \tag{9}$$

is the acoustic radius of the star; note, from equation (2), that $\Delta\nu = 1/(2T_0)$. The core phase $\delta_l(\omega)$ and the envelope phase $\alpha_l = \alpha(\omega)$ can be obtained as functions of frequency by fitting partial solutions to the oscillation equations (i.e., solutions that do not satisfy all the boundary conditions) to the relevant asymptotic expressions. In the case of α this was developed in some detail by Christensen-Dalsgaard & Pérez Hernández (1992) (see also Brodsky & Vorontsov 1988; Vorontsov & Zharkov 1989; Roxburgh & Vorontsov 1996, for a slightly different treatment of the envelope phase). As indicated, the envelope phase is independent of l for low-degree modes.

As also noted by Kallinger et al. (2012) equation (8) is clearly equivalent to equation (1), with

$$\epsilon=\frac{1}{\pi}(\alpha-\delta_0)\;, \tag{10}$$

and

$$d_{0l}=\frac{\Delta\nu}{T_0}(\delta_l-\delta_0)\;. \tag{11}$$

Equation (10) shows explicitly the contribution, through δ_0, to ϵ from the inner parts of the star. To relate $\epsilon_{\rm c}$ as defined by Kallinger et al. (2012) to the properties of ϵ we note from

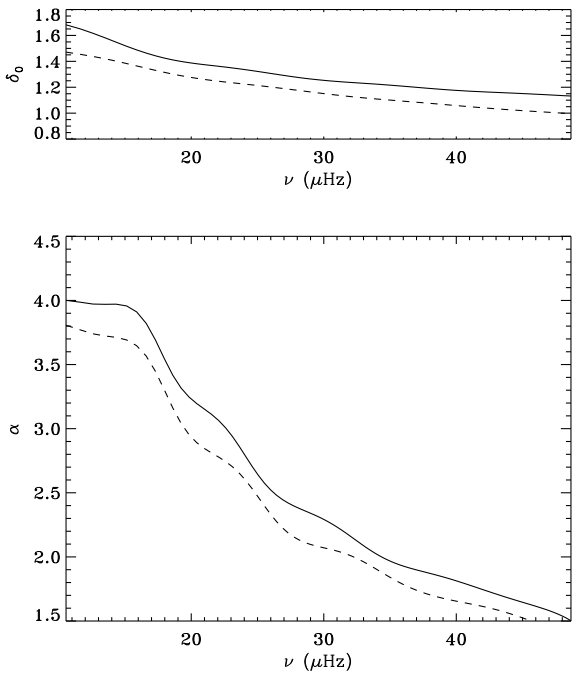

Figure 3. Core phase δ_0 for radial waves (upper panel) and envelope phase α (lower panel), as functions of frequency, for two models at the same radius. Solid lines show results for the red-giant model $\mathcal{M}_{\rm RGB}$ and dashed lines results for the clump model $\mathcal{M}_{\rm RC}$ (cf. Table 1).

equation (1), with $l = 0$ and $d_{0l} = 0$, equation (6) and equation (7), that

$$\epsilon_{\rm c}=\frac{n_{\rm c}+\epsilon(\nu_{n_{\rm c}0})}{1+[\epsilon(\nu_{n_{\rm c}+1\,0})-\epsilon(\nu_{n_{\rm c}-1\,0})]/2}\mod 1\;. \tag{12}$$

Thus $\epsilon_{\rm c}$ depends on both $\epsilon(\nu)$ and its variation with frequency.

The phase functions were determined by matching computed partial solutions to the relevant asymptotic expressions, in terms of the function

$$\psi(r)=\frac{(\rho c)^{1/2}}{r}p'\;, \tag{13}$$

where ρ is density and p' is the Eulerian pressure perturbation. In the inner part of the model the relevant form is

$$\psi_{\rm c}(r)\simeq A_{\rm c}\sin\left(\omega\tilde\tau-\pi l/2+\delta_l(\omega)\right)\;, \tag{14}$$

where $\psi_{\rm c}$ is obtained from a partial solution satisfying just the central boundary conditions; here

$$\tilde\tau=\int_0^r\frac{{\rm d}r'}{c} \tag{15}$$

is the acoustic distance to the centre. The term in l is included to acknowledge the behaviour of the solution in main-sequence stars, owing to the singular point at $r = 0$ (see Roxburgh & Vorontsov 2003). In the outer parts of the model the relevant form is

$$\psi_{\rm e}(r)\simeq A_{\rm e}\sin\left(\omega\tau-\alpha(\omega)\right)\;, \tag{16}$$

where $\psi_{\rm e}$ is obtained from a partial solution satisfying just the surface boundary conditions and

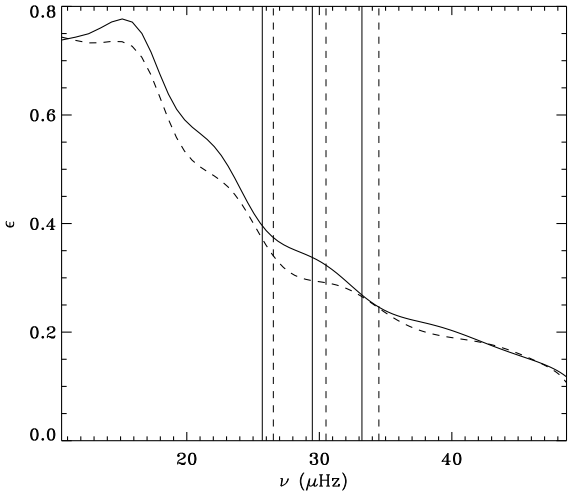

Figure 4. Combined phase ϵ as a function of frequency, for two models at the same radius. The solid line shows results for the red-giant model $\mathcal{M}_{\rm RGB}$ and the dashed line results for the clump model $\mathcal{M}_{\rm RC}$ (cf. Table 1). The solid and dashed vertical lines mark the frequencies used for determination of $\epsilon_{\rm c}$ in models $\mathcal{M}_{\rm RGB}$ and $\mathcal{M}_{\rm RC}$, respectively.

$$\tau = \int_r^{R_*} \frac{{\rm d}r'}{c} \tag{17}$$

is acoustic depth. Note that $\delta_l(\omega)$ and $\alpha(\omega)$ are defined for *any* frequency ω. The eigenfrequency equation, equation (8), follows from equations (14) and (16) by demanding that $\psi_{\rm c}$ and $\psi_{\rm e}$ represent the same solution which is continuous and with continuous first derivative at some suitable fitting point $r_{\rm f}$.

The properties of α and δ_0 and their effect on $\epsilon_{\rm c}$ can be illustrated by considering models $\mathcal{M}_{\rm RGB}$ and $\mathcal{M}_{\rm RC}$ (cf. Table 1), utilizing the fact that from equation (10) ϵ can be obtained as a continuous function of frequency. The core and envelope phases for these models are illustrated in Fig. 3 and the resulting ϵ is shown in Fig. 4; here the phases were determined by fitting the solutions to the relevant asymptotic expressions (equations 14 and 16) near $r/R = 0.75$, chosen to be below the region of varying adiabatic compressibility Γ_1 (cf. Fig. 5). Interestingly, the overall difference between the two models is similar for δ_0 and α, and hence the scale of the difference in ϵ is modest. However, there are clear differences in the frequency dependence of α and hence ϵ. This has a substantial effect on $\epsilon_{\rm c}$ through the denominator in equation (12).

To make this explicit and separate the contributions from δ_0 and α we first linearize the change in $\epsilon_{\rm c}$ in the changes in ϵ. We introduce $\epsilon_0 = \epsilon(\nu_{n_{\rm c}\,0})$, $\epsilon_+ = \epsilon(\nu_{n_{\rm c}+1\,0})$ and $\epsilon_- = \epsilon(\nu_{n_{\rm c}-1\,0})$. Then according to equation (12)

$$\epsilon_{\rm c} = \frac{n_{\rm c}+\epsilon_0}{1+(\epsilon_+-\epsilon_-)/2} \mod 1 = \frac{n_{\rm c}+\epsilon_0}{1+(\epsilon_+-\epsilon_-)/2} - n_{\rm c}\,, \tag{18}$$

where the second equality was found to be satisfied for the models considered here, or

$$\epsilon_{\rm c} = \frac{\epsilon_0 - n_{\rm c}(\epsilon_+-\epsilon_-)/2}{1+(\epsilon_+-\epsilon_-)/2}\,. \tag{19}$$

Linearizing this in small changes $\delta\epsilon$ to ϵ we obtain

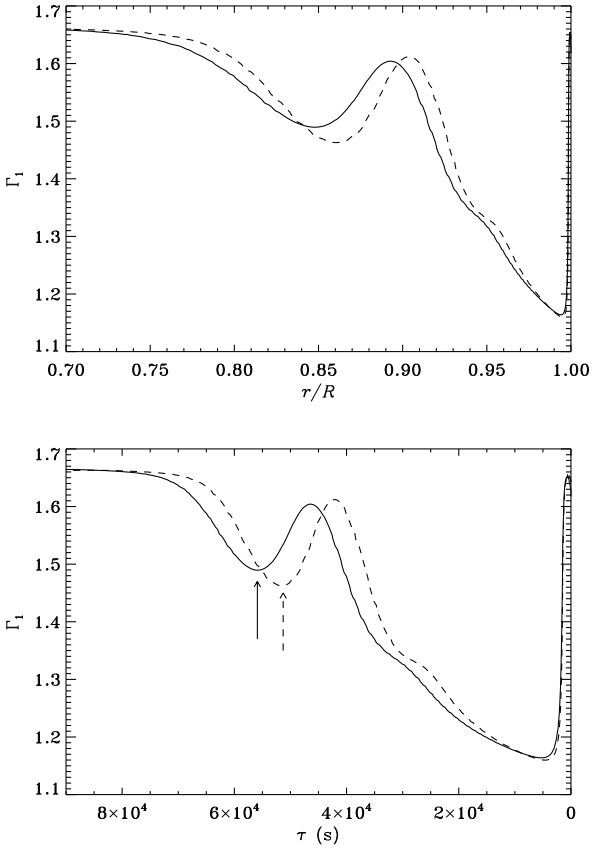

Figure 5. Adiabatic compressibility Γ_1 for two models at the same radius. The solid line shows the red-giant model $\mathcal{M}_{\rm RGB}$ and the dashed line the clump model $\mathcal{M}_{\rm RC}$ (cf. Table 1). In the upper panel Γ_1 is shown against fractional radius, while in the lower panel the abscissa is acoustic depth (cf. equation 17). The solid and dashed arrows mark the dips in Γ_1 caused by the second helium ionization in models $\mathcal{M}_{\rm RGB}$ and $\mathcal{M}_{\rm RC}$, respectively.

$$\delta\epsilon_{\rm c} \simeq \frac{\delta\epsilon_0}{1+(\epsilon_+-\epsilon_-)/2} - \frac{(\epsilon_0+n_{\rm c})(\delta\epsilon_+-\delta\epsilon_-)/2}{[1+(\epsilon_+-\epsilon_-)/2]^2}\,. \tag{20}$$

It is obvious that $\delta\epsilon = \pi^{-1}(\delta\alpha - \delta(\delta_0))$. Thus equation (20) can be used to estimate the separate contributions from the core, through $\delta(\delta_0)$, and from the envelope, through $\delta\alpha$.

Some numerical results are shown in Table 2, comparing a pair of RGB models with different $T_{\rm eff}$ (cf. Fig. 2) with the RGB and clump pair. The linearized expression in equation (20) recovers the actual difference in $\epsilon_{\rm c}$ to within 2 per cent. Also, the envelope contribution is completely dominant, by more than a factor of 6 in the RGB - clump case, thus confirming what one might have naively expected. This dominance is even stronger, obviously, for models along the sequence of RGB models with varying $\alpha_{\rm ML}$, given that in this case there is little variation in the internal structure.

To understand the origin of the strong difference in behaviour as a function of $T_{\rm eff}$ seen in Fig. 2 we note that the oscillations in ϵ as a function of frequency (cf. Fig. 4) are strongly reminiscent of the effect on the frequencies of the acoustic glitch associated with the second helium ionization zone, induced by the variation in Γ_1 (Gough 1990; Vorontsov et al. 1991; for a detailed analysis of the effects of

Table 2. Comparison of phases in two pairs of $1\,M_\odot$ models, all with radius $10.69\,R_\odot$. The central column compares two RGB models of different mixing length (cf. Fig. 2), whereas the right-hand column compares the RGB model $\mathcal{M}_{\rm RGB}$ (1) and the clump model $\mathcal{M}_{\rm RC}$ (2). The phases ϵ_c were determined from equation (12) based on the phase function $\epsilon(\nu)$, and linearized difference was obtained from equation (20), with corresponding determination of the δ (core) and α (envelope) contributions.

	RGB, varying $\alpha_{\rm ML}$	RGB, Clump
$T_{\rm eff}(1)$ (K)	4417	4417
$T_{\rm eff}(2)$ (K)	4788	4618
$\epsilon_c(1)$	0.8376	0.8376
$\epsilon_c(2)$	0.8994	0.6615
Difference	0.0618	−0.1772
Linearized difference	0.0614	−0.1801
δ contribution	−0.0008	0.0278
α contribution	0.0622	−0.2079

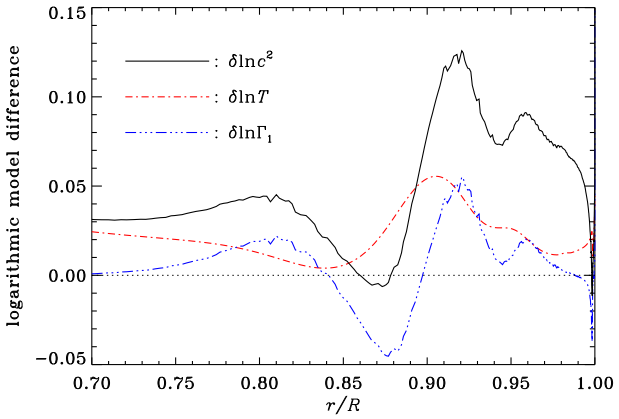

Figure 6. Differences in natural logarithm between quantities in the clump model $\mathcal{M}_{\rm RC}$ and the RGB model $\mathcal{M}_{\rm RGB}$ at fixed fractional radius, in the sense $\mathcal{M}_{\rm RC} - \mathcal{M}_{\rm RGB}$. Solid line: c^2; dot-dashed line: T; triple-dot-dashed line: Γ_1.

the helium glitch, see Verma et al. 2014). A glitch located at a depth τ_g gives rise to a variation in the frequency, and correspondingly in ϵ, of the form $\sin(2\omega\tau_g)$ and hence with a 'period' in cyclic frequency of $1/(2\tau_g)$. Fig. 5 shows Γ_1 in the two models, clearly showing that the acoustic glitch from the second helium ionization zone in the clump model is somewhat shallower in acoustic depth and of larger amplitude than in the RGB model. Correspondingly, at least in a qualitative sense, the oscillatory variation of ϵ in the clump model (cf. Fig. 4) is stronger and with a longer period than in the RGB model, causing differences in the behaviour around $\nu_{\rm max}$ and hence in ϵ_c.

As a further illustration of the origin of the different properties of ϵ_c between the clump and RGB model, Fig. 6 shows differences between these two models. The direct effect on $\epsilon(\nu)$ is undoubtedly related to the difference in c^2 which, assuming the ideal gas law and given that the composition is essentially the same, is proportional to $\Gamma_1 T$. Thus the sound-speed difference arises from the sum of the differences in T and Γ_1, with the sharp feature dominated by Γ_1, as assumed in the discussion of the glitches above. These differences arise from a difference in the thermodynamic state between the convective envelopes in the two models, related to a substantial difference in the adiabatic constant, characterized by p/ρ^{Γ_1} in the deeper parts of the convection zone. In particular, in the bulk of the convection zone the density at fixed fractional radius is lower by about a factor 0.4 in model $\mathcal{M}_{\rm RC}$, compared with model $\mathcal{M}_{\rm RGB}$. This leads to an increase in the degree of ionization in the clump model relative to the RGB model, and hence to the outward shift in the location of helium ionization, reflected in Γ_1 (cf. Fig. 5). The difference in density appears to be related to the fact that a larger fraction of the mass is contained in the compact helium core in the clump model; we discuss this in more detail in the Appendix. In the corresponding pair of RGB models with different mixing length the differences in the adiabatic constant, and other thermodynamic quantities, are minimal. The increase in the effective temperature at fixed radius, caused by the increase in the mixing length, is accompanied by a *decrease* in the temperature in the bulk of the convection zone; this is a consequence of the increase in the convective efficacy and hence a decrease in the superadiabatic temperature gradient. This leads to a shift of the second helium ionization zone to slightly greater acoustic depth, causing the modest increase in ϵ_c (cf. Fig. 2 and Table 2).

The analysis in the Appendix provides a more detailed understanding of the properties of the convective envelope and its relation to the core of the star, expressed in terms of the adiabatic constant K in the bulk of the convection zone. An interesting result is the dependence on K of the temperature and sound speed in the deeper parts of the convection zone. This appears to be related, at least in a qualitative sense, to a feature noted by Miglio et al. (2012) in fitting global asteroseismic observations for RGB and clump stars; Miglio et al. showed that differences in the sound-speed structure between these two classes of stars have a significant effect when using the scaling relation (3) in such fits.

4 DISCUSSION AND CONCLUSIONS

The properties of the phase ϵ_c, determined according to Kallinger et al. (2012) from radial modes near the frequency of maximum oscillation power, provide an interesting diagnostic to separate stars on the red-giant branch from clump stars. We have demonstrated that this effect is not a direct result of the substantial differences in core structure between these two classes of stars. Instead, it is caused by differences in the thermodynamic state of the convection zone, shifting the location in acoustic depth of the acoustic glitch caused by the second helium ionization zone. We have analysed this in terms of the phase function $\epsilon(\nu)$ which, as indicated, is defined for any frequency. The shift in the acoustic glitch causes a change in the oscillatory behaviour of ϵ and hence, as a result of the local nature of the definition used by Kallinger et al., a change in ϵ_c. The effect on ϵ of these changes in the model structure might instructively be analysed in terms of the kernels for the phase function introduced

by Christensen-Dalsgaard & Pérez Hernández (1992). We note that Vrard et al. (in preparation) fitted the variation in the separation of the radial modes as a function of frequency to take account of the glitch due to the signature of the discontinuity from the second helium ionization zone. They used the phase of this oscillatory signal as a function of $\nu_{\rm max}$ to explain the evolutionary classification based on $\epsilon_{\rm c}$ proposed by Kallinger et al. (2012). The observational approach by Vrard et al. is closely related to the theoretical analysis performed here, reaching consistent conclusions.

It is of obvious potential interest to use $\epsilon_{\rm c}$ as a diagnostic of evolutionary state for shorter data sets where the mixed modes, and hence the g-mode period spacing, cannot be obtained. We have estimated the expected uncertainty in $\epsilon_{\rm c}$ in 50-day observations, using standard error propagation, based on the scatter in the results of $\Delta\nu_{\rm c}$ obtained using the method described by Kallinger et al. (2012) for twelve 50-day datasets per star for nearly 1000 stars (Hekker et al. 2012). This expected uncertainty is typically of order 0.05 – 0.07 for stars in the frequency range of the red clump. We expect this to increase for even shorter datasets. As shown by Kallinger et al. (2012) the width of the scatter in $\epsilon_{\rm c}$ for RGB stars is of the order of 0.1 while for clump stars the spread in $\epsilon_{\rm c}$ is 0.2 to 0.3 (their Fig. 4). The value of the expected uncertainty is such that we expect a significantly larger confusion rate at the boundary of the RGB and RC as indicated by the (arbitrary) limit defined by Kallinger et al. (2012) (dotted line in their Fig. 4). This confusion has not been defined by Kallinger et al., but is expected to be (at least partly) due to larger intrinsic uncertainties caused by the stochastic excitation of the oscillations which affects results from short datasets. The estimated uncertainty is not negligible compared with the difference at fixed $\Delta\nu_{\rm c}$, of order 0.2, in $\epsilon_{\rm c}$ between the RGB and the clump stars (cf. Fig. 1 and Table 1); even so, we expect that determination of $\epsilon_{\rm c}$ from at least 50 days of observation will provide some separation between RGB and clump stars. For even shorter datasets, such as obtained over most of the sky with TESS, such a separation may be questionable but should certainly be investigated.

The variation with frequency of ϵ is directly related to the individual frequency separation $\Delta\nu_{nl}$ between modes of adjacent orders (cf. equation 4). Miglio et al. (2010) detected this variation in a red giant observed by CoRoT and used the period of the variation, reflecting the acoustic depth of the variation in Γ_1 caused by the second helium ionization zone, as a diagnostics of the stellar properties. Miglio et al. also noted that the amplitude of the variation in principle provides a measure of the envelope helium abundance, although the available data did not allow a meaningful determination. The oscillatory behaviour of the envelope phase, or various combinations based on it, have been used extensively for estimating the solar envelope helium abundance, starting with Vorontsov et al. (1991). Pérez Hernández & Christensen-Dalsgaard (1994a) pointed out that a cleaner measure could be obtained by filtering the phase function to take out the slowly varying part; this was used by Pérez Hernández & Christensen-Dalsgaard (1994b) to estimate the solar helium abundance, while Pérez Hernández & Christensen-Dalsgaard (1998) evaluated the diagnostic potential in main-sequence stars showing solar-like oscillations. Houdek & Gough (2007) investigated the diagnostics of the solar envelope on the basis of second differences of frequencies at fixed degree, to isolate the oscillatory component of the variation, and applying an asymptotic analysis of the near-surface behaviour of the oscillations to characterize the effect of the helium abundance on the seismic signature.

A detailed analysis of the potential for diagnostics of the helium ionization zone based on acoustic-mode frequencies in red giants was carried out by Broomhall et al. (2014), on the basis of fits to second differences of frequencies similar to those of Houdek & Gough (2007). Broomhall et al. noted the difficulties arising from the sparcity of the acoustically-dominated modes, and the complexity induced for dipolar modes by the mixed behaviour. Their results showed, as also found by Miglio et al. (2010), that the acoustic depth of the helium ionization could be determined reasonably reliably, whereas the amplitude of the signal, reflecting the abundance of helium, was difficult to obtain with an accuracy providing a significant abundance determination, even with the nearly four years of data provided by the *Kepler* mission. It is possible that a more detailed analysis of the envelope phase, perhaps involving the filtering proposed by Pérez Hernández & Christensen-Dalsgaard (1994a), could lead to a more robust determination of the abundance. This probably deserves further investigation.

ACKNOWLEDGEMENTS

We thank G. Houdek for useful discussions, and A. Weiss and the anonymous referee for comments on earlier versions of the manuscript which helped improving the presentation. We gratefully acknowledge the financial and organizational support from the Lorentz Center, Leiden, through the workshop 'Asteroseismology in red-giant stars', where this project was initiated. Funding for the Stellar Astrophysics Centre is provided by the Danish National Research Foundation (Grant DNRF106). The research is supported by the European Research Council through the ASTERISK project (ASTERoseismic Investigations with SONG and Kepler; Grant agreement no 267864) and the StellarAges project (Grant agreement no 338251). YE acknowledges support from the UK Science and Technology Facilities Council (STFC). This research has made use of NASA's Astrophysics Data System.

REFERENCES

Aerts C., Christensen-Dalsgaard J., Kurtz D. W., 2010, Asteroseismology, Springer, Heidelberg.
Angulo C. et al., 1999, Nucl. Phys. A, 656, 3
Baglin A., Auvergne M., Barge P., Deleuil M., Michel E. and the CoRoT Exoplanet Science Team, 2009, in Pont, F., Sasselov, D., Holman, M., eds, Proc. IAU Symp. 253, Transiting Planets, IAU and Cambridge University Press, p. 71
Beck P. G. et al., 2011, Science, 332, 205
Bedding T. R. et al., 2010, ApJ, 713, L176
Bedding T. R. et al., 2011, Nature, 471, 608
Belkacem K., Goupil M. J., Dupret M. A., Samadi R., Baudin F., Noels A., Mosser B., 2011, A&A, 530, A142

Borucki W. J. et al., 2010, Science, 327, 977
Brodsky M. A., Vorontsov S. V., 1988, in Domingo V., Rolfe E. J., eds, ESA SP-286, Seismology of the Sun and Sun-like Stars, ESA Publications Division, Noordwijk, The Netherlands, p. 487
Broomhall A.-M. et al., 2014, MNRAS, 440, 1828
Brown T. M., Gilliland R. L., 1994, ARA&A, 32, 37
Christensen-Dalsgaard J., 1984, in Mangeney A., Praderie F., eds, Space Research Prospects in Stellar Activity and Variability, Paris Observatory Press, p. 11
Christensen-Dalsgaard J., 1988, in Christensen-Dalsgaard J., Frandsen S., eds, Proc. IAU Symposium No 123, Advances in helio- and asteroseismology, Reidel, Dordrecht, p. 295
Christensen-Dalsgaard J., 1997, in Pijpers F. P., Christensen-Dalsgaard J., Rosenthal C. S., eds, SCORe'96: Solar Convection and Oscillations and their Relationship, Kluwer, Dordrecht, p. 3
Christensen-Dalsgaard J., 2008, Ap&SS, 316, 113
Christensen-Dalsgaard J., Pérez Hernández F., 1992, MNRAS, 257, 62
Christensen-Dalsgaard J., Gough D. O., Thompson M. J., 1992, A&A, 264, 518
De Ridder J. et al., 2009, Nature, 459, 398
Dupret M.-A. et al., 2009, A&A, 506, 57
Ferguson J. W., Alexander D. R., Allard F., Barman T., Bodnarik J. G., Hauschildt P. H., Heffner-Wong A., Tamanai A., 2005, ApJ, 623, 585
Gough D. O., 1990, in Osaki Y., Shibahashi H., eds, Lecture Notes in Physics, vol. 367, Progress of seismology of the sun and stars, Springer, Berlin, p. 283
Grevesse N., Sauval A. J., 1998, in Fröhlich, C., Huber, M. C. E., Solanki, S., von Steiger, R., eds, Space Science Reviews, 85, Proc. ISSI Workshop on Solar Composition and its Evolution – from Core to Corona, Kluwer, Dordrecht, p. 161
Hekker S. et al., 2012, A&A, 544, A90
Houdek G., Gough D. O., 2007, MNRAS, 375, 861
Howell S. B. et al., 2014, PASP, 126, 398
Huber D. et al., 2010, ApJ, 723, 1607
Iglesias C. A., Rogers F. J., 1996, ApJ, 464, 943
Kallinger T. et al., 2010, A&A, 509, A77
Kallinger T. et al., 2012, A&A, 541, A51
Kippenhahn R., Weigert A., Weiss A., 2012, Stellar structure and evolution, Second Edition, Springer-Verlag, Berlin
Miglio A. et al., 2010, A&A, 520, L6
Miglio A. et al., 2012, MNRAS, 419, 2077
Mosser B. et al., 2011a, A&A, 532, A86
Mosser B. et al., 2011b, A&A, 525, L9
Mosser B. et al., 2012, A&A, 540, A143
Pérez Hernández F., Christensen-Dalsgaard J., 1994a, MNRAS, 267, 111
Pérez Hernández F., Christensen-Dalsgaard J., 1994b, MNRAS, 269, 475
Pérez Hernández F., Christensen-Dalsgaard J., 1998, MNRAS, 295, 344
Ricker G. R. et al., 2014, submitted to Proc. SPIE, Astronomical Telescopes + Instrumentation. [arXiv:1406.0151v1]
Rogers F. J., Swenson F. J., Iglesias C. A., 1996, ApJ, 456, 902

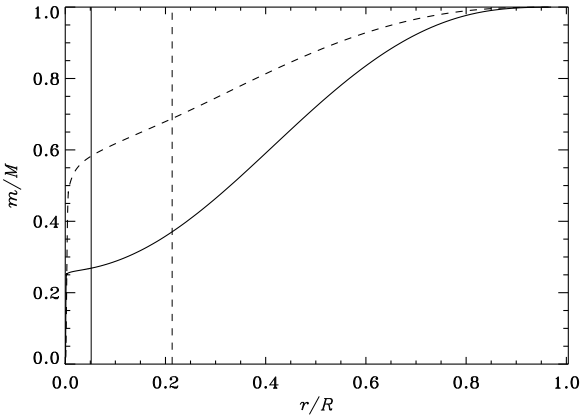

Figure A1. Fractional mass as a function of fractional radius in the RGB model $\mathcal{M}_{\rm RGB}$ (solid line) and the clump model $\mathcal{M}_{\rm RC}$ The vertical solid and dashed lines mark the base of the convective envelope in the RGB and the clump models, respectively.

Roxburgh I. W., Vorontsov S. V., 1996, MNRAS, 278, 940
Roxburgh I. W., Vorontsov S. V., 2000, MNRAS, 317, 141
Roxburgh I. W., Vorontsov S. V., 2003, A&A, 411, 215
Salaris M., Cassisi S., Weiss A., 2002, PASP, 114, 375
Silva Aguirre V. et al., 2014, ApJ, 784, L16
Stello D., Bruntt H., Preston H., Buzasi D., 2008, ApJ, 674, L53
Stello D. et al., 2014, ApJ, 788, L10
Tassoul M., 1980, ApJS, 43, 469
Ulrich R. K., 1986, ApJ, 306, L37
Verma K., Antia H. M., Basu S., Mazumdar A., 2014, ApJ, in the press, [arXiv:1408.4284]
Vorontsov S. V., Zharkov V. N., 1989, Sov. Sci. Rev. E. Astrophys. Space Phys., 7, 1
Vorontsov S. V., Baturin V. A., Pamyatnykh A. A., 1991, Nature, 349, 49
Weiss A., Schlattl H., 2008, Ap&SS, 316, 99
White T. R., Bedding T. R., Stello D., Christensen-Dalsgaard J., Huber D., Kjeldsen H., 2011, ApJ, 743, 161

APPENDIX A: PROPERTIES OF CONVECTIVE ENVELOPES

It is of obvious interest to obtain a better understanding of the differences between the RGB and clump model in the structure of the convective envelope, reflected in Fig. 6. As far as the envelope is concerned, an important difference between the models is that in the clump star a larger fraction of the mass is contained in the helium core and the deep interior, as illustrated in Fig. A1. Correspondingly, less mass is contained in the convective envelope at a given radius in the clump model, obviously corresponding to a lower density. This is made explicit in Fig. A2, showing that the density at fixed radius in model $\mathcal{M}_{\rm RC}$ is lower than in model $\mathcal{M}_{\rm RGB}$ by more than a factor 2 in much of the convective envelope; in contrast, the temperature difference is modest. It is probably this difference in density that mainly affects the ionization state of helium, leading to the differences in Γ_1 and sound speed illustrated in Fig. 6.

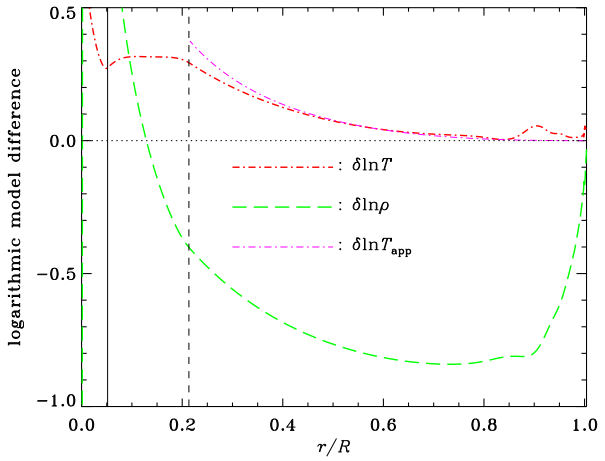

Figure A2. Differences in natural logarithm between quantities in the clump model $\mathcal{M}_{\rm RC}$ and the RGB model $\mathcal{M}_{\rm RGB}$ at fixed fractional radius, in the sense $\mathcal{M}_{\rm RC}-\mathcal{M}_{\rm RGB}$. Dashed line: ρ; dot-dashed line: T. The vertical solid and dashed lines mark the base of the convective envelope in the RGB and the clump models, respectively. The thin dot-dashed line, confined to the convective envelope in the clump model, shows the temperature difference $\delta \ln T_{\rm app}$ estimated from the approximation corresponding to equation (A11).

In the following we analyse these differences in more detail (see also, for example, Christensen-Dalsgaard et al. 1992; Christensen-Dalsgaard 1997). We note that the bulk of the convective envelope is adiabatically stratified. Neglecting furthermore the variation in Γ_1 in the ionization zones and taking $\Gamma_1 \simeq \gamma$ to be constant, p and ρ are related by

$$p = K\rho^\gamma \;, \tag{A1}$$

defining the adiabatic constant K. Introducing $u = p/\rho$, it follows from the equation of hydrostatic equilibrium,

$$\frac{{\rm d}p}{{\rm d}r} = -\frac{Gm\rho}{r^2} \;, \tag{A2}$$

where G is the gravitational constant, that

$$\frac{{\rm d}u}{{\rm d}r} \simeq -\frac{\gamma-1}{\gamma}\frac{Gm}{r^2} \;. \tag{A3}$$

In the outer parts of the convective envelope we can neglect the variation in mass and take $m \simeq M$. Then equation (A3) can be immediately integrated, to yield

$$u \simeq \frac{\gamma-1}{\gamma}\frac{GM}{R_{\rm s}}\left(\frac{R_{\rm s}}{r}-1\right) = \frac{\gamma-1}{\gamma}\frac{GM}{R_{\rm s}}\xi \;, \tag{A4}$$

where $R_{\rm s} \simeq R$ is a suitable reference radius and $\xi = R_{\rm s}/r - 1$. It follows that the squared sound speed is

$$c^2 = \gamma u \simeq (\gamma-1)\frac{GM}{R_{\rm s}}\xi \;. \tag{A5}$$

Also, assuming the ideal gas law, the temperature is approximated by

$$T \simeq \frac{\mu m_{\rm u}}{k_{\rm B}}\frac{p}{\rho} \simeq \frac{\gamma-1}{\gamma}\frac{\mu m_{\rm u}}{k_{\rm B}}\frac{GM}{R_{\rm s}}\xi \;, \tag{A6}$$

where μ is the mean molecular weight, $m_{\rm u}$ is the atomic mass unit and $k_{\rm B}$ is Boltzmann's constant. Finally, it follows from equations (A1) and (A4) that

$$\rho \simeq \rho_0 \xi^n \;, \tag{A7}$$

where $n = 1/(\gamma-1)$ is the polytropic index and

$$\rho_0 = K^{-n}\left(\frac{\gamma-1}{\gamma}\frac{GM}{R_{\rm s}}\right)^n \;. \tag{A8}$$

For the fully ionized ideal gas relevant here $\gamma = 5/3$, and hence $n = 3/2$.

In the comparison of models $\mathcal{M}_{\rm RGB}$ and $\mathcal{M}_{\rm RC}$, which have approximately the same mass and radius, equation (A6) predicts that there should be little difference in temperature. As shown in Fig. A2 this is indeed approximately the case in the outer parts of the convective envelope, although with modest differences related to variations induced by the helium ionization zone. On the other hand, equation (A7) predicts a difference $\delta \ln \rho \simeq -n\delta \ln K$, given by the difference in the adiabatic constant, which is independent of position, which again is approximately satisfied in the outer parts of the convection zone, as shown in Fig. A2.

Although moving beyond the immediate topic of the present paper it is of interest to consider the behaviour in the deeper parts of the convection zone, where the mass can no longer be considered to be constant. We write $m = M - \Delta m$, where, using equation (A7),

$$\Delta m = 4\pi\int_r^R \rho r'^2 {\rm d}r' \simeq \frac{4\pi R_{\rm s}^3}{n+1}\rho_0\xi^{n+1}\mathcal{I}_n(\xi) \;; \tag{A9}$$

here, following Christensen-Dalsgaard et al. (1992), we introduced

$$\mathcal{I}_n(\xi) = (n+1)\int_0^1 v^n(1+\xi v)^{-4}{\rm d}v \;, \tag{A10}$$

v being an integration variable, defined such that $\mathcal{I}_n(0) = 1$. Using this approximation to m in equation (A3) we obtain

$$u \simeq \frac{\gamma-1}{\gamma}\frac{GM}{R_{\rm s}}\xi\left[1 - q_0\frac{\xi^{n+1}}{n+2}\mathcal{J}_n(\xi)\right] \;, \tag{A11}$$

where

$$q_0 = \frac{4\pi R_{\rm s}^3\rho_0}{(n+1)M} \tag{A12}$$

and

$$\mathcal{J}_n(\xi) = (n+2)\int_0^1 v^{n+1}\mathcal{I}_n(v\xi){\rm d}v \;, \tag{A13}$$

which, like $\mathcal{I}_n$, is defined such that $\mathcal{J}_n(0) = 1$. Plots of $\mathcal{I}_n$ and $\mathcal{J}_n$, for $n = 3/2$, are shown in Fig. A3. Similar expressions are obviously obtained for c^2 and T. Also, from equation (A1) we obtain

$$\rho \simeq \rho_0\xi^n\left[1 - q_0\frac{\xi^{n+1}}{n+2}\mathcal{J}_n(\xi)\right]^n \;. \tag{A14}$$

It follows from equation (A11) that u, and hence c^2 and T, depend on the adiabatic constant through the term in q_0 within the brackets. This is reflected in the behaviour of $\delta \ln T$ in Fig. A2. To make a more quantitative comparison we estimated ρ_0 in the two models by applying equation (A8) at $r = 0.7R$ and determining the corresponding values of q_0 from equation (A12), resulting in $q_0 = 2.07$ and 0.89 for models $\mathcal{M}_{\rm RGB}$ and $\mathcal{M}_{\rm RC}$. Using these values in equation (A11) results in the estimate of $\delta \ln T$ shown by the thin

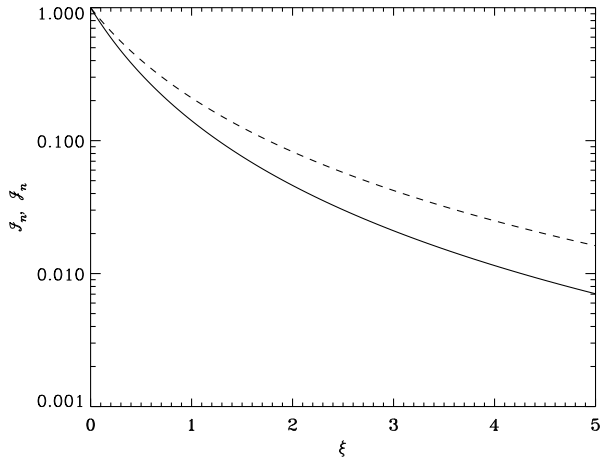

Figure A3. The functions $\mathcal{I}_n(\xi)$ (solid line) and $\mathcal{J}_n(\xi)$ (dashed line), defined by equations (A10) and (A13), for $n = 3/2$, corresponding to the value $\gamma = 5/3$ relevant for a fully ionized ideal gas.

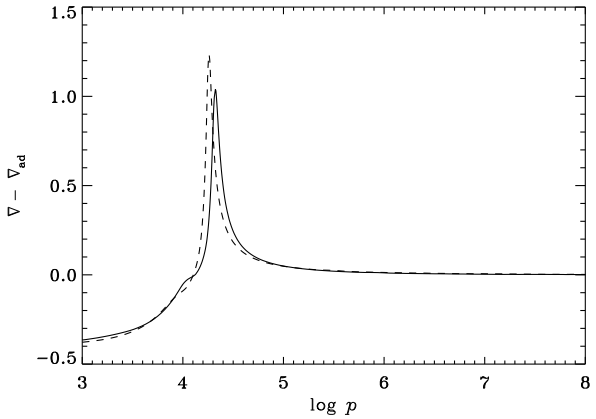

Figure A4. Superadiabatic gradient as a function of the logarithm to base 10 of pressure for models $\mathcal{M}_{\rm RGB}$ (solid line) and $\mathcal{M}_{\rm RC}$ (dashed line).

dot-dashed curve in Fig. A2. It is clear that our, relatively rough, approximation captures most of the effect on the temperature difference. Similarly, the variation in $\delta \ln \rho$ in the deeper parts of the convective envelope can be accounted for by equation (A14). It is obvious that the analysis could be iterated by repeating the determination of Δm using equation (A14); little further insight would be obtained from this, however.

The relations for the sound speed are closely related to the differences between RGB and clump stars, noted by Miglio et al. (2012), in the scaling relation for $\Delta\nu$. The integral in equation (2) is dominated by the contribution from the convective envelope. Using the approximation in equation (A5) clearly implies the commonly used scaling relation, i.e., that $\Delta\nu \propto (M/R^3)^{1/2}$. The correction factor in equation (A11) leads to a decrease in c, an increase in the integral and hence a decrease in $\Delta\nu$, relative to the simple scaling. This effect is stronger in the RGB model, owing to the larger value of q_0, than in the clump model, leading to a smaller $\Delta\nu$ in the former model at fixed mean density, as found by Miglio et al. (2012). A more quantitative analysis of this effect and its influence on the diagnostics based on global asteroseismic parameters would be interesting, but is beyond the scope of the present paper.

To relate the properties of the convective envelopes to the surface properties of the stars we note that the bulk of the convection zone is at an essentially constant specific entropy $s_{\rm ad}$, related to the adiabatic constant in the region of nearly constant Γ_1 by

$$s_{\rm ad} \simeq \frac{1}{\gamma} \ln K \; , \tag{A15}$$

apart from an arbitrary additive constant. The change in entropy between the photospheric value $s_{\rm ph}$ and $s_{\rm ad}$ is determined by the superadiabatic gradient near the top of the convection zone,

$$s_{\rm ad} = s_{\rm ph} + \int_{\ln p_{\rm ph}}^{\ln p^*} c_p (\nabla - \nabla_{\rm ad}) {\rm d} \ln p \; , \tag{A16}$$

where $\nabla = {\rm d} \ln T / {\rm d} \ln p$, $\nabla_{\rm ad}$ is its adiabatic value, c_p is the specific heat at constant pressure, $p_{\rm ph}$ is the photospheric pressure and the upper limit of the integral is at a point in the adiabatically stratified interior of the convection zone. The superadiabatic gradients in models $\mathcal{M}_{\rm RGB}$ and $\mathcal{M}_{\rm RC}$ are illustrated in Fig. A4. It is evident that $\nabla - \nabla_{\rm ad}$, and hence the integral in equation (A16), is bigger in $\mathcal{M}_{\rm RC}$ than in $\mathcal{M}_{\rm RGB}$; this dominates the fact that K is bigger in the former model, corresponding to the lower density and hence the difference in the ionization of helium leading to the difference in $\epsilon_{\rm c}$. The behaviour of ∇ in the superadiabatic region, at the assumed fixed mixing length, is dominated by the fact that the opacity is higher in model $\mathcal{M}_{\rm RC}$ than in $\mathcal{M}_{\rm RGB}$, owing to the higher effective temperature and hence higher photospheric temperature and the strong temperature dependence of the dominant H^- opacity.

This leaves open the question of the dominant causation in the difference between the thermodynamic state of the two models. It seems plausible to us that the main effect must be the higher mass in the core and the consequent lower density in the convective envelope, at fixed stellar radius. The properties of the superficial parts of the convective envelope have to respond to this, requiring the higher superadiabatic gradient and hence the higher effective temperature. Further investigations of this interplay between the interior and superficial properties of red giants appear worthwhile.